AIP | Review of Scientific Instruments

Versatile multiwavelength imaging diagnostic in the MAST spherical tokamak

A. Patel, P. G. Carolan, N. J. Conway, C. A. Bunting and R. J. Akers

Citation: Rev. Sci. Instrum. **75**, 4145 (2004); doi: 10.1063/1.1789608
View online: http://dx.doi.org/10.1063/1.1789608
View Table of Contents: http://rsi.aip.org/resource/1/RSINAK/v75/i10
Published by the American Institute of Physics.

Versatile multiwavelength imaging diagnostic in the MAST spherical tokamak

A. Patel,[a] P. G. Carolan, N. J. Conway, C. A. Bunting, and R. J. Akers
EURATOM/UKAEA Fusion Association, Culham Science Centre, Abingdon, Oxfordshire OX14 3DB, United Kingdom

(Presented on 21 April 2004; published 13 October 2004)

Spectral imaging diagnostics that view the full plasma cross section are used on MAST with sensor resolutions and frame rates of up to 256×512 chords and 130 Hz, respectively. The incident and solid angles of filter illumination are fully controllable. Image splitting and spectral selection with separate filters are performed in the telecentric region of the optics, whereas quasicontinuous polychromatic selection is achieved with a single filter in the convergent region. The versatility is investigated in exploiting the diagnostic techniques facilitated by neutral beam injection. Three color image dissection, detection of impurity charge exchange emission and Balmer-alpha beam emission are demonstrated. In another application it has been possible to use a single narrow band filter to image the spatially varying Doppler shifted emission from an inclined neutral beam even though the spatial variation well exceeds the filter bandwidth. [DOI: 10.1063/1.1789608]

I. INTRODUCTION

Building on our previous experience of imaging the MAST visible bremsstrahlung,[1] the flexibility built into the original design has now been further exploited for other applications. The narrow bandwidth capability and the wide field of view available is important in monitoring line emissions arising from the high energy neutral beam injection in MAST. These include D_α emission from the beam fast neutrals, the charge exchange neutrals and the background neutrals, as well as from Rydberg transitions in charge exchange fuel and impurity ions. The adaptations to the optics are minor to accomplish these various applications and, indeed, allowing for several to be accommodated simultaneously using a single set of viewing optics, for example. We illustrate the various methods used with results from MAST including cases where full advantage is taken of the MAST open viewing geometry and the supporting high resolution diagnostics, such as the Thomson scattering system.[2]

II. BASIC DESIGN

The diagnostic operates in the visible with a field-of-view (FOV) that views the full MAST plasma or (~48°), (see Fig. 1). This is accomplished with medium acceptance angles (f number $\geqslant$3.5). Figure 2 shows a schematic layout of the diagnostic that initially images the whole FOV onto a flat-field primary image which in turn is imaged onto a large area, frame transfer, commercial charge coupled device camera. The collection lens system has a relatively long back focal length, allowing an extensive telecentric region (chief rays parallel to the optical axis). The primary image is demagnified onto the sensor using high quality, flat field optics. The chief rays in this case are converging in a controlled manner. Telecentricity allows operations on the image while still preserving integrity. In the convergent region polychromatic selection is achieved with a tilted filter. The incorporation of convergent and telecentric regions in one design, means a cost-effective, reliable, high definition system leading to minimal use of space at the port.

III. IMAGE OPERATIONS: CONVERGENT REGION

The versatility of the diagnostic design is demonstrated in the convergent region. In the case there is a range of Doppler shifted D_α emission from a neutral particle beam due to the variable angle α to the chief ray (Fig. 3). These are then matched to the blueshift of the band pass center wavelength due to the filter tilt, given by $\lambda/\lambda_0=(1-(1/n^2)\sin^2\theta)^{1/2}$, where λ and λ_0 are the shifted and unshifted band centre wavelengths and n is the effective filter

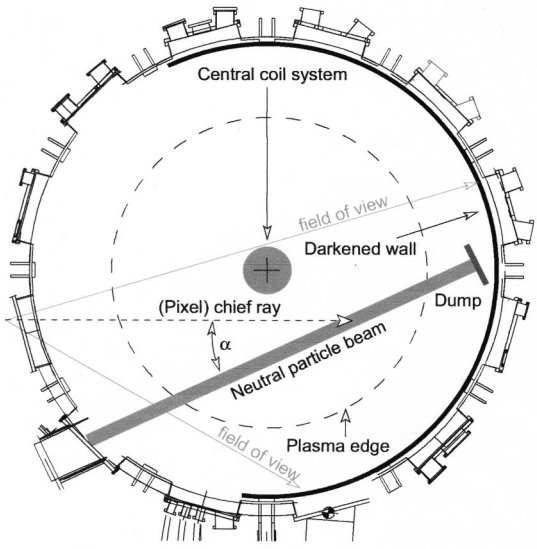

FIG. 1. Schematic diagram (plan view) of the imaging diagnostic deployment in MAST vessel (diameter ~4 m) (see Ref. 3).

[a]Electronic mail: ashwin.patel@ukaea.org.uk

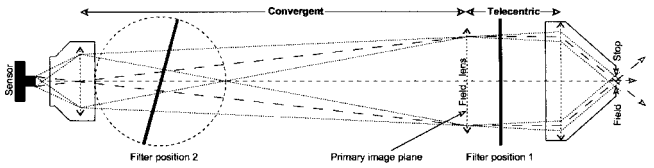

FIG. 2. Schematic diagram of the imaging diagnostic showing main optical components with possible filter positions in the telecentric and convergent sections of the design.

refractive index and θ is the chief ray angle to the filter normal. The FOV covers the full beam path in plasma. Angles made by the chief ray along the beam path ($22° < \alpha < 55°$) give varying red shifts of the primary beam energy (4–2.5 nm, respectively). Isolation of the primary energy component[4] has advantages such as rejection of the beam emission from other energy components, the reduction of bremsstrahlung, and impurity background compared with a fixed, wide spectral band pass filter. For MAST, appropriate filter specifications and tilt are chosen to track the Doppler shifts for the full range of operational primary energies (40–50 keV neutral deuterons).

IV. IMAGE OPERATIONS: TELECENTRIC REGION

The sizable back focal length permits several image operations, a selection of which are shown schematically in Fig. 4. Beam splitting in this region using a pellicle or a dichroic mirror give common views for further wavelength selection and image processing. Image dissection using plates, for example at the plasma equator, allows separation of the image, e.g., avoiding dead areas at filter edges. An example presented here, shown in Fig. 5, consists of three filters placed at the primary image plane: a thin filter (covering the equivalent of ~40% of the beam width) transmits Doppler shifted D_α emission from the main beam energy components. The upper and lower segments of the FOV contain edge-to-edge joined filters that transmit C^{5+} and He^+ Rydberg lines at 529.1 and 468.6 nm, respectively (including the charge exchange emissions from part of the beam). Results from this setup are shown elsewhere in these proceeding.[5]

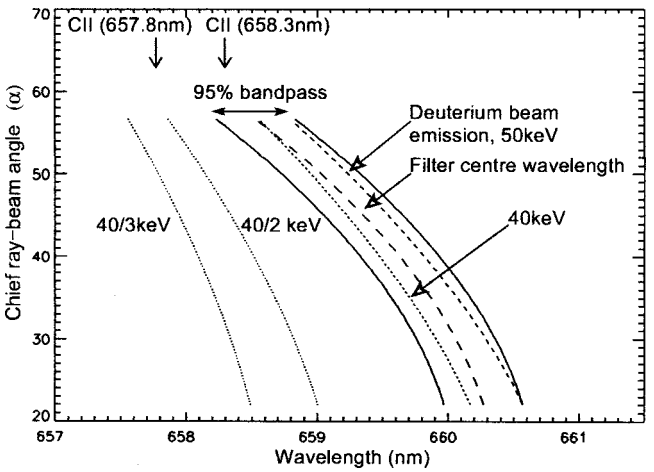

FIG. 3. Use of a single tilted narrow band filter in the convergent section to image the whole beam path in plasma, the filter bandwidth is minimized to include only the given range of Doppler shifts and the beam energies.

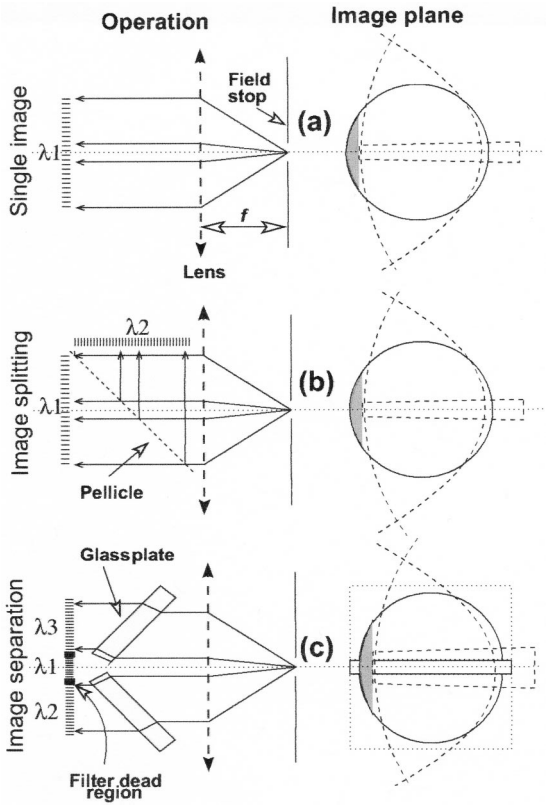

FIG. 4. Image operations in the telecentric region: (a) plain image, (b) splitting, and (c) separation.

V. VESSEL MAPPING

An important requirement of multiple imaging and profile measurement diagnostics is the absolute position calibration of the matrix viewing. This calibration is done *in situ* with a flash lamp illuminating the interior of the vacuum vessel synchronised with the imaging hardware. An example high resolution image with a tilted filter in the convergent region is shown in Fig. 6. Vessel features at the equator such as beam dump tile edges, vessel sector boundaries, etc. are

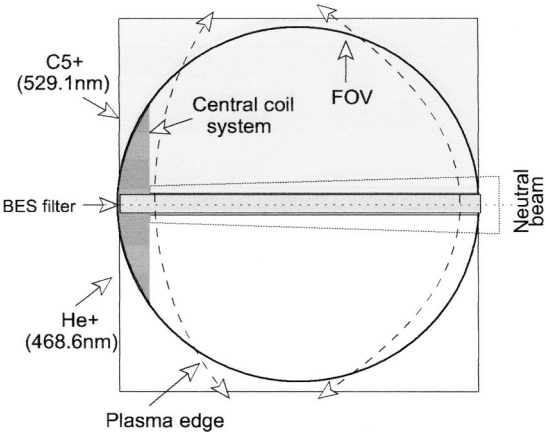

FIG. 5. Use of multiple filters at the primary image plane [cf. Fig. 4(c)].

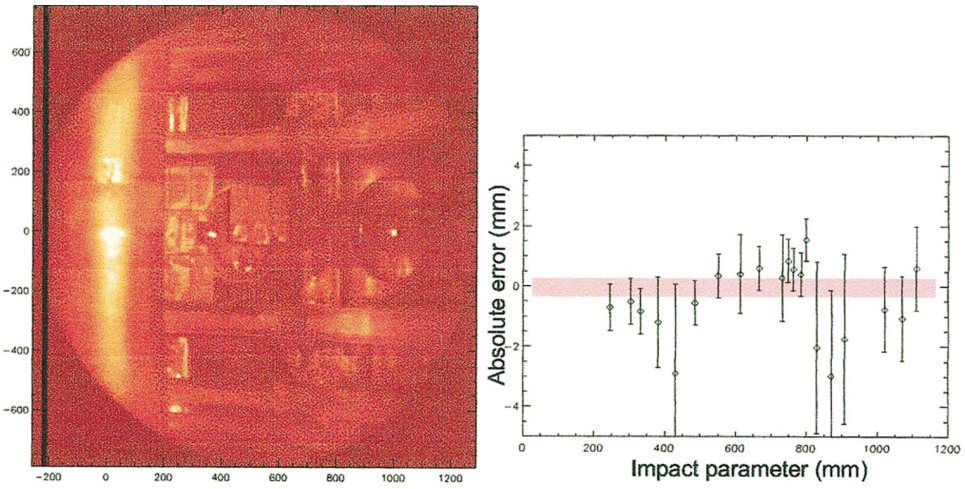

FIG. 6. (Color) Image of the MAST interior (1024×1024 pixels) showing vessel features for the tiltted filter case. Impact parameter errors at the equator are also shown after the unfolding of optical distortions.

compared with MAST engineering specifications. The agreement between the two are better than 1 mm in impact parameter. The pixel to vessel mapping process, shown here, may be repeated to other image operations mentioned in this article.

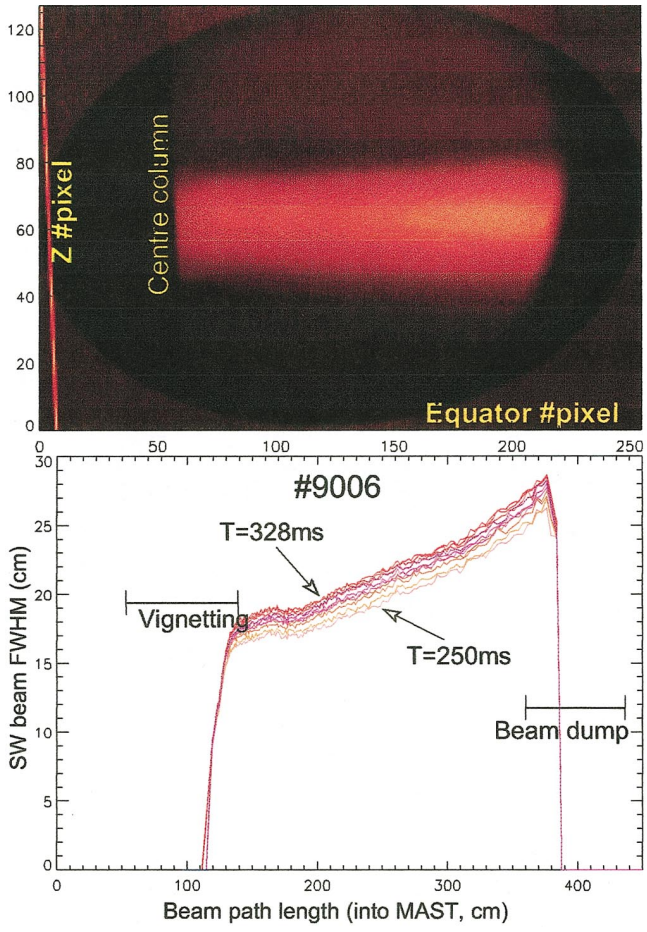

FIG. 7. (Color) Single image of the full-energy component of the neutral beam, using a gas filled vacuum vessel. The full width half maximum of the beam along its path and in time is also shown (No. 9006, 256×128, 130 Hz).

VI. BEAM PRIMARY ENERGY IMAGING

Results shown in this section include absolute spatial intensity calibrations of the diagnostic using a large area (high FOV) integrating sphere. Spectral sensitivity across the FOV may be checked using an integrating sphere-spectrometer combination.

An unattenuated beam, for the case of the beam into a gas filled vessel, is shown in Fig. 7. The temporal evolution of the primary energy beam width as a function of path length for one beam period is shown in Fig. 7—the divergence along the path and temporally is as expected. A beam into plasma case is shown in Fig. 8 and shows good agreement with a model of the beam attenuation that is based on

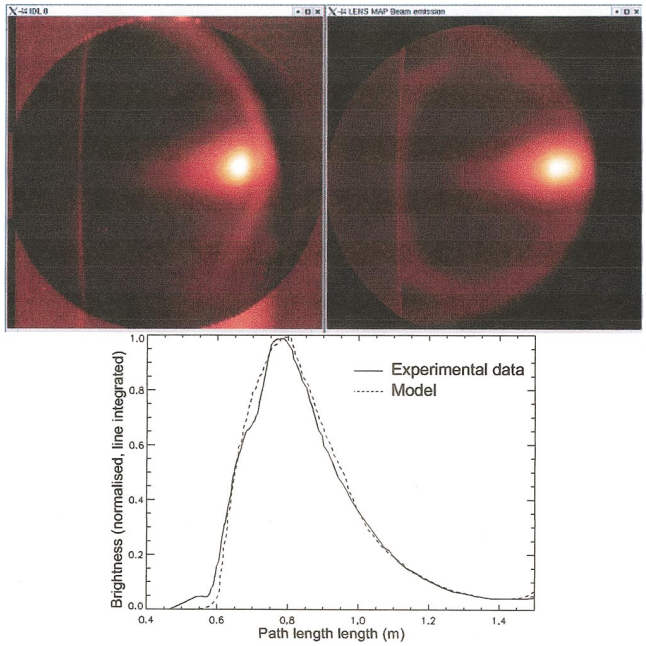

FIG. 8. (Color) Beam into plasma (No. 9000): comparison of a single 256×256 pixel time frame (left) with a model generated image (right). The lower part compares the axial data with model estimated intensities.

experimentally measured quantities (density, temperature, and Z_{eff}) and beam stopping/emission rate coefficients.

ACKNOWLEDGMENTS

The authors would like to thank M. J. Walsh for a seminal discussion also K. Hawkins for technical contributions. This work was funded jointly by the United Kingdom Engineering and Physical Sciences Research Council and by EURATOM.

[1] A. Patel, P. Carolan, N. Conway, and R. Akers, Rev. Sci. Instrum. (submitted for publication).
[2] M. J. Walsh, E. R. Arends, P. G. Carolan, M. R. Dunstan, M. J. Forrest, S. K. Nielsen, and R. O'Gorman, Rev. Sci. Instrum. **74**, 1663 (2003).
[3] A. Sykes *et al.*, Phys. Plasmas **8**, 2101 (2001).
[4] S. Fielding and D. Stork, Nucl. Fusion **22**, 617 (1982).
[5] P. Carolan, Rev. Sci. Instrum. these proceedings.